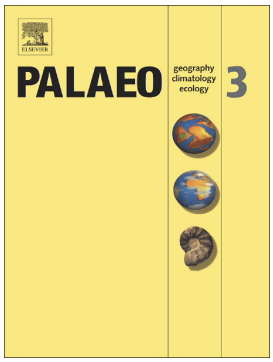

Reconstructed springtime (March–June) precipitation tracked by tree rings dating back to 1760 CE in the Qinling-Bashan mountainous area

Shijie Wang, Wenmin Man, Feng Chen, Youping Chen, Shulong Yu, Honghua Cao, Mao Hu, Tiyuan Hou, Martín A. Hadad, Fidel A. Roig

PII: S0031-0182(22)00381-9

DOI: https://doi.org/10.1016/j.palaeo.2022.111211

Reference: PALAEO 111211

To appear in: *Palaeogeography, Palaeoclimatology, Palaeoecology*

Received date: 6 June 2022

Revised date: 21 August 2022

Accepted date: 21 August 2022

Please cite this article as: S. Wang, W. Man, F. Chen, et al., Reconstructed springtime (March–June) precipitation tracked by tree rings dating back to 1760 CE in the Qinling-Bashan mountainous area, *Palaeogeography, Palaeoclimatology, Palaeoecology* (2022), https://doi.org/10.1016/j.palaeo.2022.111211

Reconstructed springtime (March-June) precipitation tracked by tree rings dating back to 1760 CE in the Qinling-Bashan mountainous area

Shijie Wang[1], Wenmin Man[2], Feng Chen[*1, 3], Youping Chen[1], Shulong Yu[3], Honghua Cao[1], Mao Hu[1], Tiyuan Hou[1], Martín A. Hadad[4], Fidel A. Roig[5,6]

[1] *Yunnan Key Laboratory of International Rivers and Transboundary Eco-Security, Institute of International Rivers and Eco-Security, Yunnan University, Kunming* 650500, *China*

[2] *State Key Laboratory of Numerical Modeling for Atmospheric Sciences and Geophysical Fluid Dynamics (LASG), Institute of Atmospheric Physics, Chinese Academy of Sciences, Beijing* 100029, *China*

[3] *Key Laboratory of Tree-ring Physical and Chemical Research of China Meteorological Administration/Xinjiang Laboratory of Tree-ring Ecology, Institute of Desert Meteorology, China Meteorological Administration, Urumqi* 830002, *China*

[4] *Laboratorio de Dendrocronología de Zonas Áridas CIGEOBIO (CONICET-UNSJ), Gabinete de Geología Ambiental (INGEO-UNSJ), San Juan, Argentina*

[5] *Laboratorio de Dendrocronología e Historia Ambiental, IANIGLA-CCT CONICET-Universidad Nacional de Cuyo, Mendoza, Argentina*

[6] *Hémera Centro de Observación de la Tierra, Escuela de Ingeniería Forestal, Facultad de Ciencias, Universidad Mayor, Huechuraba, Santiago, Chile*

* Corresponding author at: Institute of International Rivers and Eco-Security, Yunnan University, Kunming 650500, China

E-mail addresses: feng653@163.com (F. Chen)

ABSTRACT

In recent decades, considerable advances have been made in dendroclimatic reconstruction in the eastern monsoon region of China. However, understanding of long-term hydroclimatic changes has not been comprehensive due to the complexity of the regional geography in China's north-south transitional zone. Growth-climate response analysis indicated that springtime precipitation is the main factor limiting the radial growth of pine trees in the Qinling-Bashan mountainous area. Based on the three tree ring chronologies distributed in the southeast of Shaanxi Province, we developed a March-June precipitation reconstruction spanning 1760-2020 CE for the Qinling-Bashan mountainous area. Precipitation reconstruction accounts for 40.6% of the total precipitation variance during the instrumental period 1955-2016. Spatial correlation analysis indicated that the precipitation reconstruction recorded similar common precipitation signals for the eastern Qinling Mountains and the Yangtze-Huai River Basin. The results of the superposed epoch analysis (SEA) revealed that low precipitation was one of the main causes of severe drought and locust plague events. The preliminary synoptic climatology analysis showed that our reconstructed precipitation is closely linked to the El Niño-Southern Oscillation (ENSO) and Indian Ocean Dipole (IOD) variability.

Keywords: Qinling-Bashan mountainous area; Tree rings; Precipitation reconstruction; Drought; Locust plague; Synoptic analysis

1. Introduction

Precipitation is one of the stable and sustainable sources of freshwater resources, and is an important factor for social prosperity and ecosystem stability, especially in many developing Asian countries with more population and agricultural production (Al-Amin and Ahmed, 2016; Xia et al., 2017; Pokhrel et al., 2021). In China, water resources are extremely unevenly distributed in spatial and temporal patterns, especially in the eastern monsoon region (Xia, 2012). Due to the economic and social prosperity of the region, the sustainability of water resources has attracted increasing attention. Understanding the regional precipitation variation is of great significance for suitable water resource management (Meko and Woodhouse, 2005; Cook et al., 2010). Although efforts are made to promote the rational allocation of water resources, our understanding of the long-term regional water cycle mechanism since the instrumental climate data only cover the past few decades.

Due to their high annual resolution, long temporal coverage, and annual accuracy, tree rings represent a valuable climate proxy indicator for understanding past climatic and hydrological variations (e.g., Cook et al., 2016; Büntgen et al., 2016; Xu et al., 2019a; Shang et al., 2020; Pearson et al., 2020; Chen et al., 2021a). During the past two decades, several tree-ring chronologies have been developed for climate reconstruction in the monsoon region of eastern China (e.g., Xu et al., 2013; Cai and Liu, 2017; Zhao et al., 2019; Chen et al., 2020; Chen et al., 2021b), including the Qinling Mountains and Huai River regions. This geographic feature divide China's monsoon zone into north and south, showing distinct natural and cultural conditions (e.g., Hughes et al., 1994; Garfin et al., 2005; Liu et al., 2009; Chen et al., 2013, 2016;

Yang et al., 2016; Hu et al., 2018; Zhao et al., 2019; Zheng et al., 2021). However, previous reconstructions have mainly focused on the connection to north-central China, while few studies have showed the similarity in the Yangtze-Huai River region. Due to the complex mountainous terrain and spatial differences in the local climate of the Qinling-Bashan mountainous area in China's north-south transitional zone, it is necessary to develop further precipitation reconstructions to interpret the past drought variation.

China has been a primarily agricultural country since ancient times, with cultivated land and grain production ranked among the highest in the world. Agricultural disasters have occurred frequently throughout history, causing serious economic losses, especially by drought and locust plague (Zhai, 2005; Zhang, 2008; Tian et al., 2011). Tree-ring records can provide support for related studies on agriculture and climate in the past (Stahle et al., 2012; Chen et al., 2022), but they still lack in the eastern China. Concurrently, these disasters are often related to extreme climate variation, which has been linked to sea surface temperature, especially in the monsoon region. Wu et al. (2003) and Sun et al. (2021) found that El Niño-Southern Oscillation (ENSO) events profoundly affected the subsequent precipitation in eastern China, which was characterized by an increase in precipitation in the south and a decrease in the north during El Niño years, while the opposite was found during La Niña years. Zhang et al. (2022) emphasized the influence of the Indian Ocean Dipole (IOD) on precipitation in eastern China and analyzed the similarities and differences with ENSO. Therefore, it is necessary to deepen the analysis of the influence of

precipitation variation on agricultural disasters and the causes of extreme precipitation events from a long-term perspective.

In this study, we present a March-June precipitation reconstruction spanning 1760-2020 CE in the Qinling-Bashan mountainous area. This precipitation reconstruction was conducted using a composite tree-ring growth chronology from *Pinus bungeana* and *Pinus tabuliformis* applying three sites across southeastern Shaanxi Province. The precipitation reconstruction will be of great significance to multiple water resource management planning and high-quality economic and social development. Therefore, the purposes of our study are as follows: (1) to analyze the response of the composite chronology to climate factors; (2) to reconstruct precipitation and analyze its variation; (3) to analyze the spatial correlation pattern and compare it with other reconstructions; (4) to study the effects of precipitation on drought and locust plague; and (5) to explore the synoptic climatological causes involved in extreme precipitation events.

2. Materials and methods

2.1. Study area

Our study region is located at the east of the Qinling-Bashan mountainous area, which is in the China's north-south transitional zone (Fig. 1a). Surrounded by the Wei River, Han River, Huai River, Yellow River, and Yangtze River, the region has abundant water resources and has made great contributions to China's water supply system, such as the South-to-North Water Transfer Project (Li et al., 2015). The study

area is part of the eastern monsoon region of China and the east of Hu line (Hu, 1935), with a dense population and developed economy (Fig. 1b). Controlled by the Asian monsoon system, the precipitation and temperature reach their peaks during the summer and early autumn periods. Data from Shangxian meteorological station during 1955-2016 show that the annual average precipitation is 695.5 mm, and the annual average temperature is 12.9 ℃, showing a weak downward and upward trend respectively (Fig. 2.b, d). It is noteworthy that the interdecadal variation in precipitation is more significant than the average temperature (Fig. 2.a, c).

2.2. Sampling and chronology development

As two of the dominant tree species in our study region, *Pinus bungeana* and *Pinus tabulaeformis* are very sensitive to climate variation. Tree-ring samples (WXS, DLS, and HPC) were collected from three sites in southeastern Shaanxi Province, China (Fig. 1; Table 1). Cores of WXS were sampled in Wuxian village, Shangluo City in 2018. Cores of DLS were sampled in Dalao mountain, Shangluo City in 2018. Cores of HPC were sampled in Huaiping village, Ankang City in 2020. Table 1 lists the site information of the three sites, including latitude and longitude, elevation, and cores/trees. To obtain better regional climate signals, we selected shallow or rocky soil of open forests for sampling and only selected healthy trees. For the most suitable trees, we used increment borers to sample two cores of each tree from different directions at breast height. In total 133 tree-ring cores were collected at the three sampling sites.

After being fixed and air-dried naturally, all newly collected samples were

uniquely numbered and sanded smooth. The width of each tree ring was measured at a resolution of 0.001 mm with the CDendro 9.4 analysis system and proofread with the software TSAP-Win. The quality of cross-dating was controlled by the results of COFECHA software, which uses correlation analysis to check the dating reliability (Holmes, 1983). COFECHA results showed that the mean intercorrelation of the ring-width series from the WXS chronology was 0.575, with an average mean sensitivity of 0.349 and a probability of absent rings of 0.351%. In the other DLS (HPC) chronology, the results were 0.471 (0.436), 0.306 (0.295), 0.375% (0.639%), respectively. The tree-ring growth chronology was developed with a bi-weight robust mean method using the ARSTAN program (Cook, 1985). To remove undesirable growth trends linked to age, we chose the negative exponential functions and Friedman smoothing curves to standardize the data (Cook, 1985; Yamaguchi and Cook, 1991). Since the residual chronology (RES) yielded the strongest correlation with instrumental March-June precipitation, we used the RES chronology for our final reconstruction. In addition, the expressed population signal (EPS, Wigley et al., 1984) was computed to obtain the reliable part of the composite chronology. The composite chronology applied in the reconstruction dated back to 1760 CE, as the EPS value reached 0.85 and the sample depth reached 10 cores (Fig. 3a). The composite chronology has high statistical eigenvalues, such as the mean sensitivity and signal-to-noise ratio, indicating the common environmental influence on the radial growth of trees (Table 2). Meanwhile, the correlation coefficients between the composite chronology and the three chronologies (WXS, DLS, and HPC) are 0.785,

0.538, and 0.563 respectively; the first-order differential correlation coefficients are 0.805, 0.605, and 0.691 respectively. The significant correlations indicate that the composite chronology can capture the common high and low frequency changes of all tree-ring cores.

2.3 Data and analysis

The monthly climate data (1955-2016) were obtained from the Shangxian meteorological station, which is the closest climate station, with no data gaps. The relationships between tree growth and climate factors were analyzed from the previous July to the current November (17 months) by Pearson correlation analysis (Blasing et al., 1984). A simple linear regression equation was established for precipitation reconstruction. To examine the dependability and applicability of the reconstruction model, we conducted a split-sample calibration-verification test, including the correlation coefficient (r_1), explained variance (R^2), correlation coefficient of the first difference (r_2), product mean test (PMT), F test (F), reduction of error (RE) and average coefficient of efficiency (CE) (Cook et al., 1999). The coefficient of variation (CV) was used to describe the degree of discreteness of instrumental and reconstructed precipitation.

To remove the interannual signal and obtain the long-term chronological signal, we smoothed our precipitation reconstruction through the low-pass filtering method for 15 years. The wet (dry) periods were identified if the smoothed values were higher (lower) than the overall mean without a break for exceeding 9 years (≥ 9 years) (Li et al., 2022). A single value lower than 2 standard deviations (SDs) compared to the

average value was recognized as an extremely low precipitation year. The 10-year average value and cumulative anomaly curve were also used to eliminate outliers and determine the continuous variation characteristics of precipitation. The multitaper spectral analysis method (MTM) was used to calculate the principal cycles of the precipitation reconstruction (Therrell et al., 2006).

Superposed epoch analysis (SEA; Haurwitz and Brier, 1981) was applied to analyze the response of major drought and locust plague events in relation to precipitation variations. If the events occurred, they were recorded as zero years. At the same time, the variations 6 years before and after the event year were tested. In the case of multidecadal composites of drought or locust plague, we used 15-year low-pass filtered precipitation reconstruction and only selected the 10 strongest event years (Wang et al., 2017). An event year was not selected if it was close to another event year. For every multidecadal composite, the 95% confidence interval was determined as the composite mean ± 2 SDs.

We calculated the spatial correlation patterns between the reconstructed precipitation and gridded data, including the 0.5°×0.5° gridded precipitation (CRU TS 4.05; Harris et al., 2014) and standardized precipitation evapotranspiration index (CSIC SPEI; Beguería et al., 2014). In addition, we considered the sea surface temperature (SST) from the HadISST dataset (Rayner et al., 2003). The water vapor analysis was carried out using the Community Earth System Model Last Millennium Ensemble (CESM-LME) simulation (Otto-Bliesner et al., 2016). CESM-LME data were obtained by coupling the atmosphere, ocean, land surface, sea ice, and land ice

through CESM1.1, with a resolution of 2°×2°. We used the all-forcing multi-model ensemble average of 10 members for analysis to eliminate the randomness of individual members. Several studies have proved the rationality of the influence of CESM-LME on large-scale circulation in eastern China (Zhou and Jiang, 2021; Xue et al., 2022). To reveal the causes of extreme precipitation, the SST anomalies from the previous December to current June during 1870-2020 were composited. Furthermore, we analyzed the impact of ENSO and IOD on precipitation and 850 hPa water vapor transport anomalies during 1760-2005 in the CESM-LME simulation. For the selection of ENSO event years, we used the calculation method of the ONI provided by the National Oceanic and Atmospheric Administration (NOAA), which is the moving average of SST anomaly in Nino 3.4 area (5°S-5°N, 120°W-170°W) for three consecutive months. For the selection of IOD event years, we used the calculation method of the DMI provided by Saji et al. (1999), which is the difference between the SST anomaly of the tropical West Indian Ocean (10°S-10°N, 50°E-70°E) and the equatorial southeast Indian Ocean (10°S-0°, 90°W-110°W).

3. Results

3.1. Precipitation reconstruction

The results of the climate response showed that tree-ring growth overall was positively correlated with precipitation and negatively correlated with temperature (Fig. 3b). Significant positive correlations ($p < 0.05$) with the precipitation occurred in the current March ($r = 0.268$), April ($r = 0.313$), and May ($r = 0.398$), and significant

negative correlations ($p < 0.05$) with the temperature occurred in the current May (r = -0.432) and June (r = -0.292). After correlation analysis with different monthly combinations, the composite chronology responded most positively to total March-June precipitation (r = 0.637, $p < 0.001$), and responded most negatively to mean May-June temperature (r = -0.483, $p < 0.001$). Physiologically, total March-June precipitation is the critical climate variable in the Qinling-Bashan mountainous area, affecting water availability and hence the radial growth of pine trees. Therefore, we developed total March-June precipitation reconstruction for the Qinling-Bashan mountainous area since 1760 CE.

The transfer model was developed as follows:

$$Y = 31.543 + 202.6X$$

where X is the composite chronology and Y is the total March-June precipitation reconstruction (mm).

The CV of the instrumental precipitation was 0.275, while the CV of the reconstructed precipitation was only 0.176. Except for the size of some extreme values, the reconstructed precipitation fit well with the instrumental precipitation on the inter-annual scale (Fig. 3c, d). The reconstruction explained 40.6% of the actual March-June precipitation variation from 1955 to 2016. Meanwhile, at high-frequency comparisons, the correlation coefficient of the first-order differences was 0.753. The results of the split verification test indicated that the reconstruction was reliable (Table 3). The values of RE and CE were strongly positive, and r_1, r_2, PMT and F were all found at the 0.01 significance level, which indicates the validity of our reconstruction

model. Therefore, the final reconstruction of the total precipitation from March to June for the Qinling-Bashan mountainous area extended from 1760 to 2020 CE.

3.2. Characteristics of precipitation reconstruction

The springtime (March-June) precipitation reconstruction provided important information about precipitation variations (Fig. 4a). The precipitation reconstruction spanned 261 years (1760-2020). The mean precipitation was 232.2 mm and the standard deviation (SD) was 37.8 mm. The precipitation reconstruction included 9 continuous wet periods (1760-1775, 1779-1787, 1832-1843, 1859-1873, 1882-1896, 1905-1922, 1935-1955, 1965-1978, 1988-1996), and 7 continuous dry periods (1788-1799, 1808-1818, 1844-1854, 1923-1934, 1956-1964, 1979-1987, 1997-2013) (Fig. 4b; Table 4). Extremely low precipitation years (< 156.5 mm) occurred in 1786, 1795, 1821, 1835, 1847, 1857, 1901, 1929, and 2007. At the same time, the cumulative anomaly curve and the 10-year average showed that the precipitation reconstruction fluctuated but was higher, after experiencing significantly low values in the early 19th century and the early 20th century. Subsequently, it showed low values at approximately 2000 CE (Fig. 4b). MTM analysis indicated interannual cycles of 2-5 years (Fig. 5).

The precipitation reconstruction showed a clear connection ($P < 0.05$) with the March-June gridded precipitation from 1901 to 2020 over a vast geographical area, especially in the eastern Qinling Mountains and the Yangtze-Huai River Basin (Fig. 6a). Similar spatial correlation patterns appeared between the reconstructed precipitation and SPEI from 1901 to 2018 (Fig. 6b). After extracting the large-scale

precipitation and SPEI data of the eastern Qinling Mountains and the Yangtze-Huai River Basin (28°-36° N, 108°-118° E), we find good consistency with our reconstructed precipitation (Figure 6c, d; r = 0.336/0.386, n = 120/118, $p < 0.001$). After obtaining the chronological signals through 10-year low-pass filtering, the change trends were basically consistent since 1960, a period covered by instrumental climate data. These results indicated that our precipitation reconstruction was able to capture drought signals in eastern China, especially in the China's north-south transitional zone.

Our precipitation reconstruction was compared with other's precipitation reconstructions based on tree rings in the eastern Qinling Mountains and the Yangtze-Huai River Basin (Fig. 7). The correlation coefficients between our reconstruction and Chen et al. (2016; 2013) in the Qinling Mountains are 0.341 ($p < 0.01$) and 0.226 ($p < 0.01$), respectively. There are also consistent variations between our study and the precipitation reconstruction (Xu et al., 2019b) in the Yangtze-Huai River Basin (r = 0.209, p = 0.007). The correlation between our precipitation reconstruction and the precipitation reconstruction in the south of the Yangtze River (Shi et al., 2015) has declined to some extent (r = 0.121, p = 0.130). In conclusion, our reconstruction can capture a wide range of common precipitation signals, mainly in the eastern Qinling Mountains and the Yangtze-Huai River Basin. After crossing the Yangtze River southward, the correlation decreased to some extent.

4. Discussion

4.1. Growth-climate response and regional drought variation

The tree-ring growth showed positive correlation with precipitation and negative correlation with temperature, indicating that tree-ring growth is affected by drought variations in the Qinling-Bashan mountainous area. The significant correlations were concentrated in the early growing season. Narrower tree rings are formed under higher temperature and less precipitation conditions, while wider tree rings are formed under lower temperature and more precipitation conditions (Zhao et al., 2019; Gao et al., 2021). The SPEI showed a similar or even more significant spatial correlation (Fig. 6.b), which can directly reflect the dry and wet variations by considering precipitation and temperature. During the early growing season, water deficiency can limit the expansion of cambium cells and the opening of leaf pores, inhibiting the radial growth of trees (Fritts, 1976). Evaporation increases due to higher temperatures, exacerbating the existing water deficiency. As the sampling sites and meteorological station are located in the eastern Qinling Mountains, the altitude gradually decreases eastward. Therefore, the eastern Qinling mountains may have similar circulation patterns to the Yangtze-Huai River Basin, and thus have consistent precipitation changes (Ping et al., 2014).

At the same time, our reconstruction is highly correlated with other tree ring-based precipitation reconstructions in the eastern Qinling Mountains and the Yangtze-Huai River Basin (Fig. 7). After smoothing through 15-year low-pass filtering, seven common dry periods occurred in 1776-1779, 1808-1818, 1849-1855, 1901-1905, 1923-1932, 1961-1965, and 1997-2008. The comparison of

reconstructions showed that the drought events in 1808-1818, 1923-1932, and 1997-2008 were the worst since 1760 CE, which covered a wider region. From 1811 to 1814 CE, a severe drought occurred in eastern and central China, lasting eight years in some places (Tan, 2013). The extreme drought in the late 1920s led to unprecedented disasters, including severe famine and death (Zhai, 2005; Chen et al., 2013). In the early 21st century, the drought trend occurred in Qinling-Bashan mountainous region (Liu et al., 2019; Gao et al., 2021), but water conservancy projects and artificial regulation reduced losses to a certain extent (Lu et al., 2016; Xu et al., 2020). In summary, our reconstruction captured broader regional precipitation variation, and it is of great significance to understand the long-term drought variations in these regions.

4.2. Linkage with drought and locust plague

The lack of spring precipitation often leads to agricultural disasters and grain reduction, especially in China, which is a large agricultural and populous country. We used the superposed epoch analysis (SEA) for precipitation reconstruction through 30 drought events and 30 locust plague events recorded throughout history. The lists of the drought and locust plague years, based on historical documents were used for tests. Drought events were selected from "*Chinese Meteorological Disasters Ceremony (Shaanxi Volume)*" (Zhai, 2005), which are located near the sampling sites and describe severe droughts. Locust plague events were selected from "*History of Locust Plague in China*" (Zhang, 2008), which outbroke in summer and autumn and the levels were 2 or above. Due to locust migration and high frequency of locust attacks,

we chose locust plague events in the eastern Qinling Mountains and the Yangtze-Huai River Basin.

The results indicated that precipitation was significantly lacking in drought and locust plague years (Fig. 8a, c). The results of the multidecadal composites also found a lack of precipitation (Fig. 8b, d), where prolonged absences of precipitation led to air and soil moisture deficiency, providing the conditions of magnitude droughts (Chen and Sun, 2015; Jiang and Wang, 2021). Lower precipitation increased the places suitable for locusts to lay eggs and provided plants with less water, resulting in greater viability and fecundity (Tian et al., 2011). Precipitation decreased by an average of 22.9% in drought years, while it decreased by an average of 11.9% in locust plague years (Table 5). The lack of precipitation was one of the causes of large-scale drought and locust plague events, which further led to famine. Therefore, a disaster chain of "climate-drought/locust-famine" has been formed, causing population reduction and social unrest (Kong et al., 2017). The most serious example was observed from 1928 to 1931, when extremely low precipitation led to the simultaneous outbreak of severe drought and locust plague events, leading to countless deaths and recessions. Tree-ring records provide evidence of the possible role of climatic variations in the outbreak of drought and locust plagues.

4.3. Synoptic climatology analysis of extreme precipitation years

To reveal the climatic driving force of extreme precipitation events, we synthesized the SST of the 10 wettest and driest years during 1870-2020 (Fig. 9a, b). As the winter SST change plays an important role in the East Asian precipitation for

the following year (Wang et al., 2000; Wu et al., 2003), we selected the December-June SST for analysis. The results of composite maps showed that ENSO and IOD are the causal mechanisms of precipitation variation in the Qinling-Bashan mountainous area. The rise in SST in the equatorial eastern Pacific and the Indian Ocean occurred in the wettest years, while the opposite occurred in the driest years. The 2-5 year cycles of precipitation reconstruction are also similar to the cycles of ENSO and IOD.

According to the average December-June ONI and DMI in CESM-LME, we synthesized the precipitation and 850 hPa water vapor transport anomaly maps of the strongest 10 years respectively. The results of the CESM-LME simulation (Fig. 9c-f) indicated that ENSO and IOD played important roles in water vapor transport in the Qinling-Bashan mountainous area. In El Niño and warm IOD years, with the southward movement of the Western Pacific subtropical high and the increase in water vapor in the Indian Ocean, the precipitation in the study area and the Yangtze-Huai River Basin increased (Zhang et al., 1999; Wu et al., 2003; Zhang et al., 2022). In La Niña and cold IOD years, in contrast, the rain belt moved northwards and the water vapor in the Indian Ocean weakened, resulting in less precipitation in the study area (Zhao et al., 2011; Sun et al., 2021). Some studies have shown that the frequency of extreme ENSO and IOD events increases with global warming (Cai et al., 2014; 2021), which may lead to an increase in the frequency of extreme precipitation events in the study area. Overall, one of the vital driving forces for the complex water vapor transport in the Qinling-Bashan mountainous area is large-scale

ocean-atmosphere-land circulation systems.

5. Conclusion

Based on tree rings from three sampling sites in southeastern Shaanxi Province, China, we established a composite tree-ring width chronology, which allowed us to reconstruct the springtime (March-June) precipitation variations in the Qinling-Bashan mountainous area since 1760 CE. The reconstructed precipitation experienced 9 and 7 continuous wet and dry periods, respectively, determining that the main cycles occur with a frequency of 2-5 years.

As shown in our study, precipitation variations are related to the eastern Qinling Mountains and the Yangtze-Huai River Basin but not only to the north-central China. At the same time, the reconstruction also provides evidence of droughts and locust plagues, both linked to climatic change processes. The decrease in precipitation constitutes an important link in the generation of environmental disasters. Our analyses indicate the intimate linkage of regional precipitation variation in the Qinling-Bashan mountainous area with some large-scale climate forcing, such as the ENSO and IOD.

However, our precipitation reconstruction needs to be improved as it is based on only three sample sites, covering the last 260 years and restricted to a small region. Therefore, it is of vital importance to continue developing systematic precipitation reconstructions in the Chinese monsoonal region. These efforts will provide better estimates to recognize the long-term changing characteristics of the climate and atmospheric circulation patterns that affect water availability, essential elements for the

sustainable management of water resource.

Acknowledgements. This research was supported by the National Natural Science Foundation of China (32061123008).

REFERENCES

Al-Amin, A.Q., Ahmed, F., 2016. Food security challenge of climate change: an analysis for policy selection. futures. 83, 50-63. https://doi.org/10.1016/j.futures.2016.04.002.

Blasing, T.J., Solomon, A.M., Duvick, D.N., 1984. Response function revisited. Tree Ring Bull. 44, 1-15.

Beguería, S., Vicente-Serrano, S., Reig, F., Latorre, B., 2014. Standardized precipitation evapotranspiration index (SPEI) revisited: Parameter fitting, evapotranspiration models, tools, datasets and drought monitoring. Int. J. Climatol. 34(10), 3001-3023. https://doi.org/10.1002/joc.3887.

Büntgen, U., Myglan, V.S., Ljungqvist, F.C., McCormick, M., Di Cosmo, N., Sigl, M., Jungclaus, J., Wagner, S., Krusic, P.J., Esper, J., Kaplan, J.O., de Vaan, M.A.C., Luterbacher, J., Wacker, L., Tegel, W., Kirdyanov, A.V., 2016. Cooling and societal change during the Late Antique Little Ice Age from 536 to around 660 AD. Nat. Geosci. 9(3), 231-236. https://doi.org/10.1038/ngeo2652.

Cai, Q.F., Liu, Y., 2017. Two centuries temperature variations over subtropical southeast China inferred from Pinus taiwanensis Hayata tree-ring width. Clim. Dyn. 48(5-6), 1813-1825. https://doi.org/10.1007/s00382-016-3174-8.

Cai, W.J., Borlace, S., Lengaigne, M., van Rensch, P., Collins, M., Vecchi, G., Timmermann, A., Santoso, A., McPhaden, M.J., Wu, L.X., Englan, M.H., Wang, G.J., Guilyardi, E., Jin, F.F., 2014. Increasing frequency of extreme El Niño events due to greenhouse warming. Nat. Clim. Change. 4(2), 111-116. https://doi.org/10.1038/nclimate2100.

Cai, W.J., Yang, K., Wu, L.X., Huang, G., Santoso, A., Ng, B., Wang, G.J., Yamagata, T., 2021. Opposite response of strong and moderate positive Indian Ocean Dipole to global warming. Nat. Clim. Change. 11(1), 27-32. https://doi.org/10.1038/s41558-020-00943-1

Chen, D., Zhou, F.F., Dong, Z.P., Zeng, A.Y., Du, T.H., Fang, K.Y., 2020. A tree-ring δ18O based reconstruction of East Asia summer monsoon over the past two centuries. PLoS ONE. 15(6), e0234421. https://doi.org/10.1371/journal.pone.0234421.

Chen, F., Gagen, M.H., Zhang, H.L., Chen, Y.P., Fan, Z.A., Chen, F.H., 2021b. Warm season temperature in the Qinling Mountains (north-central China) since 1740 CE recorded by tree-ring maximum latewood density of Shensi fir. Clim. Dyn. 57(9-10), 2653-2667. https://doi.org/10.1007/s00382-021-05827-4.

Chen, F., Opala-Owczarek, M., Khan, A., Zhang, H.L., Owczarek, P., Chen, Y.P., Ahmed, M., Chen, F.H., 2021a. Late twentieth century rapid increase in high Asian seasonal snow and glacier-derived streamflow tracked by tree rings of the upper Indus River basin. Environ. Res. Lett. 16(9), 094055. https://doi.org/10.1088/1748-9326/ac1b5c.

Chen, F., Yuan, Y.J., Trouet, V., Buntgen, U., Esper, J., Chen, F.H., Yu, S.L., Shen, M.G., Zhang, R.B., Shang, H.M., Chen, Y.P., Zhang, H.L., 2022. Ecological and societal effects of Central Asian streamflow variation over the past eight centuries. npj Clim. Atmos. Sci. 5(1), 27. https://doi.org/10.1038/s41612-022-00239-5.

Chen, F., Yuan, Y.J., Wei, W.S., Fan, Z.A., Yu, S.L., Zhang, T.W., Zhang, R.B., Shang, H.M., Qin, L., 2013. Reconstructed precipitation for the north-central China over the past 380 years and its linkages to East Asian summer monsoon variability. Quat. Int. 283, 36-45. https://doi.org/10.1016/j.quaint.2012.05.047.

Chen, F., Zhang, R.B., Wang, H.Q., Qin, L., Yuan, Y.J., 2016. Updated precipitation reconstruction (AD 1482–2012) for Huashan, north-central China. Theor. Appl. Climatol. 123(3-4), 723-732. https://doi.org/10.1007/s00704-015-1387-0.

Chen, H.P., Sun, J.Q., 2015. Changes in drought characteristics over China using the standardized precipitation evapotranspiration index. J. Clim. 28(13), 5430-5447. https://doi.org/10.1175/JCLI-D-14-00707.1.

Cook, B.I., Anchukaitis, K.J., Touchan, R., Meko, D.M., Cook, E.R., 2016. Spatiotemporal drought variability in the Mediterranean over the last 900years. J. Geophys. Res.-Atmos. 121(5), 2060-2074. https://doi.org/10.1002/2015JD023929.

Cook, E.R., 1985. A time series analysis approach to tree ring standardization. Tucson: University of Arizona.

Cook, E.R., Anchukaitis, K.J., Buckley, B M., D'Arrigo, R.D., Jacoby, G.C., Wright,

W.E., 2010. Asian monsoon failure and megadrought during the Last Millennium. Science. 328(5977), 486-489. https://doi.org/10.1126/science.1185188.

Cook, E.R., Meko, D.M., Stahle, D.W., Cleaveland, M.K., 1999. Drought reconstructions for the continental United States. J. Clim. 12(4), 1145-1162. https://doi.org/10.1175/1520-0442(1999)012<1145:DRFTCU>2.0.CO;2.

Fritts, H.C., 1976: Tree-Rings and Climate. London: Academic Press, 567pp.

Gao, Z.H., Chen, F., Fang, K.Y., 2021. Runoff reconstruction for the Bailong River from tree rings back to AD 1601, reveals changing hydrological signals of China north-south transition zone. Hydrol. Process. 35(11), e14417. https://doi.org/10.1002/hyp.14417.

Garfin, G.M., Hughes, M.K., Yu, L., Burns, J.M., Touchan, R., Leavitt, S.W., Zhisheng, A., 2005. Exploratory temperature and precipitation reconstructions from the Qinling Mountains, north-central China. Tree-Ring Res. 61(2), 59-72. https://doi.org/10.3959/1536-1098-61.2.59.

Harris, I., Jones, P.D., Osborn, T.J., Lister, D.H., 2014. Updated high-resolution grids of monthly climatic observations–the CRU TS3. 10 Dataset. Int. J. Climatol. 34(3), 623-642. https://doi.org/10.1002/joc.3711.

Haurwitz, M.W., Brier, G.W., 1981. A critique of the superposed epoch analysis method: its application to solar–weather relations. Mon. Weather Rev. 109(10), 2074-2079.

https://doi.org/10.1175/1520-0493(1981)109<2074:ACOTSE>2.0.CO;2.

Holmes, R.L., 1983. Computer assisted quality control in tree-ring dating and

measurement. Tree-Ring Bull. 43, 69-78. http://hdl.handle.net/10150/261223.

Hu, H.Y., 1935: The distribution of population in China, with statistics and maps. Acta Geogr. Sin. 2(2), 33-74. (in Chinese)

Hu, Y.F., Bao, G., Liu, N., Qu, Y., 2018. May-July mean minimum temperature variability in the mid-Qinling Mountains, central China, since 1814 CE. Quat. Int. 476, 102-109. https://doi.org/10.1016/j.quaint.2018.02.012.

Hughes, M. K., Xiangding, W., Xuemei, S., Garfin, G. M., 1994. A preliminary reconstruction of rainfall in north-central China since AD 1600 from tree-ring density and width. Quat. Res. 42(1), 88-99. https://doi.org/10.1006/qres.1994.1056

Jiang, D.B., Wang, X.X., 2021. A brief interpretation of drought change from IPCC Sixth Assessment Report. J. Atmos. Sci. 44(5), 650-653. https://doi.org/10.13878/j.cnki.dqkxxb.20210810007. (in Chinese)

Kong, D.Y., 2017: Research on geography of locust plague in North China Plain and its adjacent areas during 960-1949AD. Xi'an: Northwest University. (in Chinese)

Li, L.C., Zhang, L.P., Xia, J., Gippel, C.J., Wang, R.C., Zeng, S.D., 2015. Implications of modelled climate and land cover changes on runoff in the middle route of the south to north water transfer project in China. Water Resour. Manag. 29(8), 2563–2579. https://doi.org/10.1007/s11269-015-0957-3.

Li, Q., Deng, Y., Wang, S.J., Gao, L.L., Gou, X.H., 2022. A half-millennium perspective on recent drying in the eastern Chinese Loess Platea. Catena. 212, 106087. https://doi.org/10.1016/j.catena.2022.106087.

Liu, N., Bao, G., Liu, Y., Linderholm, H.W., 2019. Two centuries-long streamflow reconstruction inferred from tree rings for the middle reaches of the Weihe River in Central China. Forests. 10(3), 208. https://doi.org/10.3390/f10030208.

Liu, Y., Linderholm, H.W., Song, H.M., Cai, Q.F., Tian, Q.H., Sun, J.Y., Chen, D.L., Simelton, E., Seftigen, K., Tian, H., Wang, R.Y., Bao, G., An, Z., 2009. Temperature variations recorded in Pinus tabulaeformis tree rings from the southern and northern slopes of the central Qinling Mountains, central China. Boreas. 38(2), 285-291. https://doi.org/10.1111/j.1502-3885.2008.00065.x.

Lu, Y.J., Yan, D.H., Qin, T.L., Song, Y.F., Weng, B.S., Yuan, Y., Dong, G.Q., 2016. Assessment of drought evolution characteristics and drought coping ability of water conservancy projects in Huang-Huai-Hai River basin, China. Water. 8(9), 378. https://doi.org/10.3390/w8090378.

Meko, D.M., Woodhouse, C.A., 2005. Tree-ring footprint of joint hydrologic drought in Sacramento and Upper Colorado river basins, western USA. J. Hydrol. 308(1-4), 196-213. https://doi.org/10.1016/j.jhydrol.2004.11.003.

Otto-Bliesner, B.L., Brady, E.C., Fasullo, J., Jahn, A., Landrum, L., Stevenson, S., Rosenbloom, N., Mai, A., Strand, G., 2016. Climate Variability and Change since 850 CE: An Ensemble Approach with the Community Earth System Model, Bull. Amer. Meteorol. Soc. 97(5), 735-754. https://doi.org/10.1175/BAMS-D-14-00233.1.

Pearson, C., Salzer, M., Wacker, L., Brewer, P., Sookdeo, A., Kuniholm, P., 2020. Securing timelines in the ancient Mediterranean using multiproxy annual

tree-ring data. Proc. Natl. Acad. Sci. U. S. A. 117(31), 18891-18891. https://doi.org/10.1073/pnas.2013168117.

Ping, F., Tang, X.B., Gao, S.T., Luo, Z.X., 2014. A comparative study of the atmospheric circulations associated with rainy-season floods between the Yangtze and Huaihe River Basins. Sci. China: Earth Sci. 57(7), 1464-1479. https://doi.org/10.1007/s11430-013-4802-3.

Pokhrel, Y., Felfelani, F., Satoh, Y., Boulange, J., Burek, P., Gädeke, A., Gerten, D., Gosling, S.N., Grillakis, M., Gudmundsson, L., Hanasaki, N., Kim, H., Koutroulis, A., Liu, J.G., Papadimitriou, L., Schewe, J., Schmied, H.M., Stacke, T., Telteu, C.E., Thiery, W., Veldkamp, T., Zhao, F., Wada, Y., 2021. Global terrestrial water storage and drought severity under climate change. Nat. Clim. Chang. 11(3), 226-233. https://doi.org/10.1038/s41558-020-00972-w.

Rayner, N.A., Parker, D.E., Horton, E.B., Folland, C.K., Alexander, L.V., Rowell, D.P., Kent, E.C., Kaplan, A., 2003. Global analyses of sea surface temperature, sea ice, and night marine air temperature since the late nineteenth century. J. Geophys. Res.-Atmos. 108(D14), 4407. https://doi.org/10.1029/2002jd002670.

Stahle, D.W., Burnette, D.J., Diaz, J.V., Heim, R.R., Fye, F.K., Paredes, J.C., Soto, R.A., Cleaveland, M.K., 2012. Pacific and Atlantic influences on Mesoamerican climate over the past millennium. Clim. Dyn. 39(6), 1431-1446. https://doi.org/10.1007/s00382-011-1205-z.

Saji, N.H., Goswami, B.N., Vinayachandran, P.N., Yamagata, T., 1999. A dipole mode in the tropical Indian Ocean. Nature. 401(6751), 360-363.

https://doi.org/10.1038/43854.

Shang, H.M., Chen, F., Wei, W.S., Mao, W.Y., Zhang, R.B., Zhang, T.W., Yu, S.L., 2020. A 602-year Reconstruction of July-June Streamflow in the Kuqa River, China, Reveals the Changing Hydrological Signals of the Tarim Basin. Acta Geol. Sin.-Engl. Ed. 94(3), 690-697. https://doi.org/10.1111/1755-6724.14532.

Shi, J.F., Lu, H.Y., Li, J.B., Shi, S.Y., Wu, S.Y., Hou, X.Y., Li, L.L., 2015. Tree-ring based February-April precipitation reconstruction for the lower reaches of the Yangtze River, southeastern China. Glob. Planet. Change. 131, 82-88. https://doi.org/10.1016/j.gloplacha.2015.05.006.

Sun, L.Y., Yang, X.Q., Tao, L.F., Fang, J.F., Sun, X.G., 2021. Changing impact of ENSO events on the following summer rainfall in eastern China since the 1950s. J. Clim. 34(20), 8105-8123. https://doi.org/10.1175/JCLI-D-21-0018.1.

Tan, X.M., 2013: Historical archives of droughts in Qing dynasty. Beijing: China Books Publishing House, 1079pp. (in Chinese)

Therrell, M.D., Stahle, D.W., Ries, L.P., Shugart, H.H., 2006. Tree-ring reconstructed rainfall variability in Zimbabwe. Clim. Dyn. 26(7-8), 677-685. https://doi.org/10.1007/s00382-005-0108-2.

Tian, H.D., Stige, L.C., Cazelles, B., Kausrud, K.L., Svarverud, R., Stenseth, N.C., Zhang, Z.B., 2011. Reconstruction of a 1,910-y-long locust series reveals consistent associations with climate fluctuations in China. Proc. Natl. Acad. Sci. U. S. A. 108(35), 14521-14526. https://doi.org/10.1073/pnas.1100189108.

Wang, B., Wu, R.G., Fu, X.H., 2000. Pacific-East Asian teleconnection: how does

ENSO affect East Asian climate? J. Clim. 13(9), 1517-1536. https://doi.org/10.1175/1520-0442(2000)013<1517:PEATHD>2.0.CO;2.

Wang, J.L., Yang, B., Ljungqvist, F.C., Luterbacher, J., Osborn, T.J., Briffa, K.R., Zorita, E., 2017. Internal and external forcing of multidecadal Atlantic climate variability over the past 1,200 years. Nat. Geosci. 10(7), 512-517. https://doi.org/10.1038/ngeo2962.

Wigley, T.M., Briffa, K.R., Jones, P.D., 1984. On the average value of correlated time series, with applications in dendroclimatology and hydrometeorology. J. Appl. Meteorol. Climatol. 23(2), 201-213. https://doi.org/10.1175/1520-0450(1984)023<0201:OTAVOC>2.0.CO;2

Wu, R.G., Hu, Z.Z., Kirtman, B.P., 2003. Evolution of ENSO-Related Rainfall Anomalies in East Asia. J. Clim. 16(22), 3742-3758. https://doi.org/10.1175/1520-0442(2003)016<3742:EOERAI>2.0.CO;2.

Xia, J., 2012. Special Issue: Climate Change Impact on Water Security & Adaptive Management in China introduction. Water Int. 37(5), 509-511. https://doi.org/10.1080/02508060.2012.729176.

Xia, J., Duan, Q.Y., Luo, Y., Xie, Z.H., Liu, Z.Y., Mo, X.G., 2017. Climate change and water resources: Case study of eastern monsoon region of China. Adv. Clim. Chang. Res. 8(2), 63-67. https://doi.org/10.1016/j.accre.2017.03.007.

Xu, A.N., Yang, L.E., Yang, W.B., Chen, H., 2020. Water conservancy projects enhanced local resilience to floods and droughts over the past 300 years at the Erhai Lake basin, Southwest China. Environ. Res. Lett. 15(12): 125009.

https://doi.org/10.1088/1748-9326/abc588.

Xu, C.X., An, W.L., Wang, S.Y.S., Yi, L., Ge J.Y., Nakatsuka, T., Sano, M., Guo, Z.T., 2019a. Increased drought events in southwest China revealed by tree ring oxygen isotopes and potential role of Indian Ocean Dipole. Sci. Total Environ. 661, 645-653. https://doi.org/10.1016/j.scitotenv.2019.01.186.

Xu, C.X., Shi, J.F., Zhao, Y.S., Nakatsuka, T., Sano, M., Shi, S.Y., Guo, Z.T., 2019b. Early summer precipitation in the lower Yangtze River basin for AD 1845–2011 based on tree-ring cellulose oxygen isotopes. Clim. Dyn. 52(3-4), 1583-1594. https://doi.org/10.1007/s00382-018-4212-5.

Xu, C.X., Zheng, H.Z., Nakatsuka, T., Sano, M., 2013. Oxygen isotope signatures preserved in tree ring cellulose as a proxy for April-September precipitation in Fujian, the subtropical region of southeast China. J. Geophys. Res.-Atmos. 118(23), 12805-12815. https://doi.org/10.1002/2013JD019803.

Xue, J., Ning, L., Liu, Z.Y., Qin, Y.M., Chen, K.F., Yan, M., Liu, J., Wang, L.L., Li, C.X., 2022. The combined influences of Solar Radiation and PDO on Precipitation over Eastern China during the last millennium. Clim. Dyn. https://doi.org/10.1007/s00382-022-06372-4.

Yamaguchi, D.K., Cook, E.R., 1991. Methods of dendrochronology, applications in the environmental sciences. Arct. Alp. Res. 23(1), 120. https://doi.org/10.2307/1551446.

Yang, F., Wang, N.A., Shi, F., Ljungqvist, F.C., Zhao, S., Liu, T., 2016. The spatial distribution of precipitation over the West Qinling region, China, AD 1470-2000.

Paleogeogr. Paleoclimatol. Paleoecol. 443, 278-285. https://doi.org/10.1016/j.palaeo.2015.12.003.

Zhai, Y.A., 2005: Chinese Meteorological Disasters Ceremony (Shaanxi Volume). Beijing: China Meteorological Press, 211pp. (in Chinese)

Zhang, R.H., Sumi, A., Kimoto, M., 1999. A diagnostic study of the impact of El Niño on the precipitation in China. Adv. Atmos. Sci. 16(2), 229-241. https://doi.org/10.1007/BF02973084.

Zhang, Y., Zhou, W., Wang, X., Wang, X., Zhang, R.H., Li, Y.N., Gan, J.P., 2022. IOD, ENSO, and seasonal precipitation variation over Eastern China. Atmos. Res. 270, 106042. https://doi.org/10.1016/j.atmosres.2022.106042.

Zhang, Y.H., 2008: History of Locust Plague in China. Hefei: Anhui people's Publishing House, 442pp. (in Chinese)

Zhao, S.S., Zhou, T.J., Yang, X.Q., Zhu, Y.M., Tan, Y.K., Sun, X.G., 2011. Interdecadal change of the relationship between the tropical Indian ocean dipole mode and the summer climate anomaly in China. Acta Meteorol. Sin. 25(2), 129-141. https://doi.org/10.1007/s13351-011-0021-z.

Zhao, Y.S., Shi, J.F., Shi, S.Y., Ma, X.Q., Zhang, W.J., Wang, B.W., Sun, X.G., Lu, H.Y., Brauning, A., 2019. Early summer hydroclimatic signals are captured well by tree-ring earlywood width in the eastern Qinling Mountains, central China. Clim. Past. 15(3), 1113-1131. https://doi.org/10.5194/cp-15-1113-2019.

Zheng, Z.Y., Jin, L.Y., Li, J.J., Chen, J. Zhang, X.J., Wang, Z.Q., 2021. Moisture variation inferred from tree rings in north central China and its links with the

remote oceans. Sci. Rep. 11(1), 16463. https://doi.org/10.1038/s41598-021-93841-1.

Zhou, X.C., Jiang, D.B., 2021. A modeling analysis of East Asian summer monsoon changes on interdecadal and centennial timescales during the last millennium. Quat. Sci. 41(2), 522-535. (in Chinese)

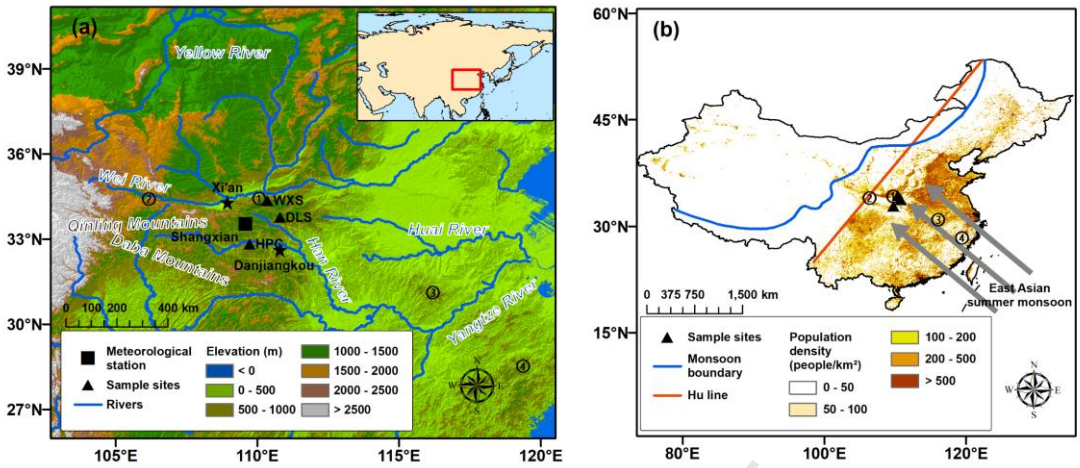

Fig. 1. (a) Locations of the tree-ring sampling sites and meteorological station. (b) Population density map of China in 2020. The positions 1, 2, 3, and 4 indicate the tree-ring sites of Chen et al. 2016, 2013, Xu et al. 2019b, and Shi et al. 2015, respectively.

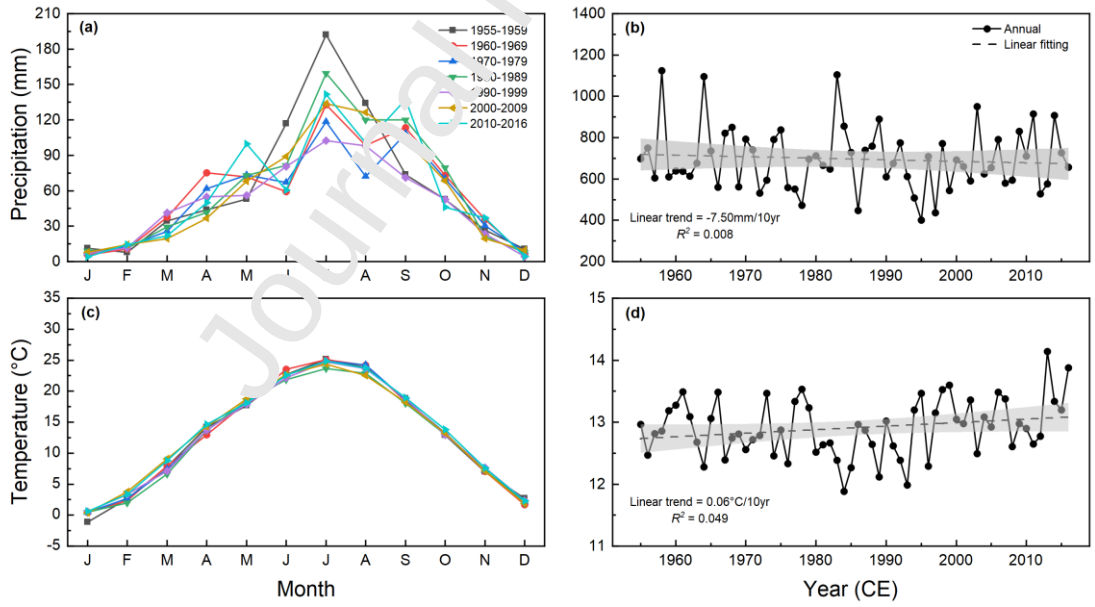

Fig. 2. Monthly decadal and annual climatic data from Shangxian meteorological station for the period 1955-2016. The legends in (c) and (d) are the same as (a) and (b) respectively. The grey shadow represents the 95% confidence level.

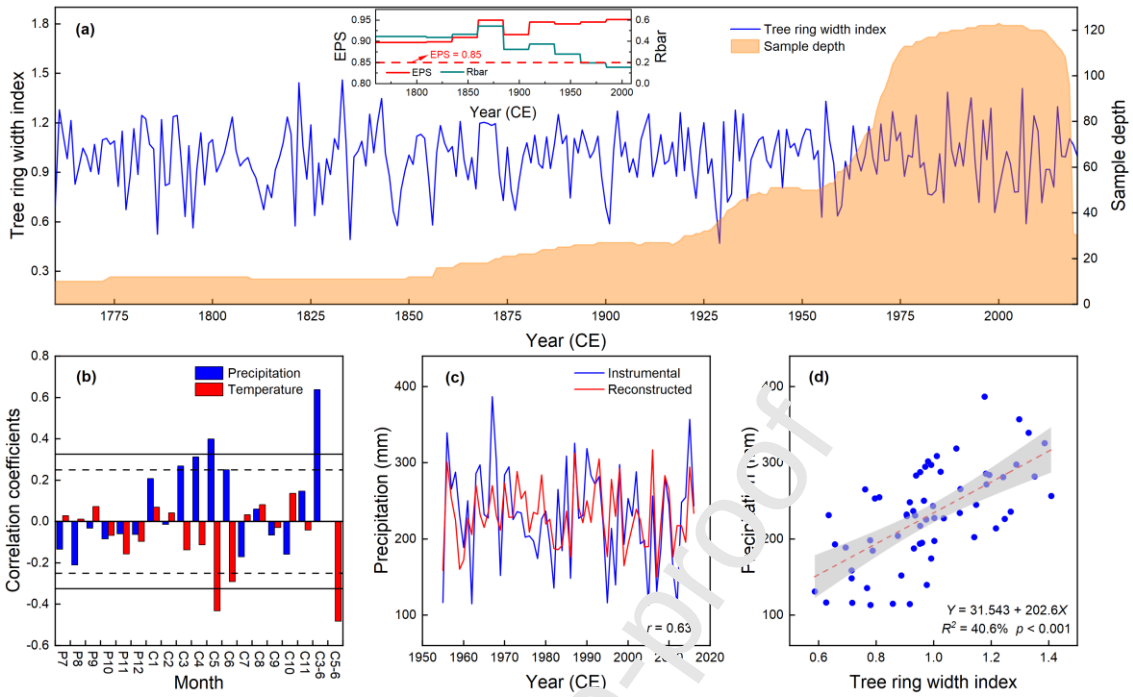

Fig. 3. (a) Tree-ring width residual chronology and sample depth. Running expressed population signal (EPS) and correlation coefficient (Rbar) statistics are shown in the inset. (b) Correlation analyses of the composite chronology with climatic factors from the previous July to the current November during 1955-2016. The solid and dashed lines represent the 99% and 95% confidence levels, respectively. (c) Comparison between the instrumental and reconstructed precipitation from March to June during 1955-2016. (d) Scatter plot of the composite chronology and the total March-June precipitation with a linear fitting curve. The shadow represents the 95% confidence level.

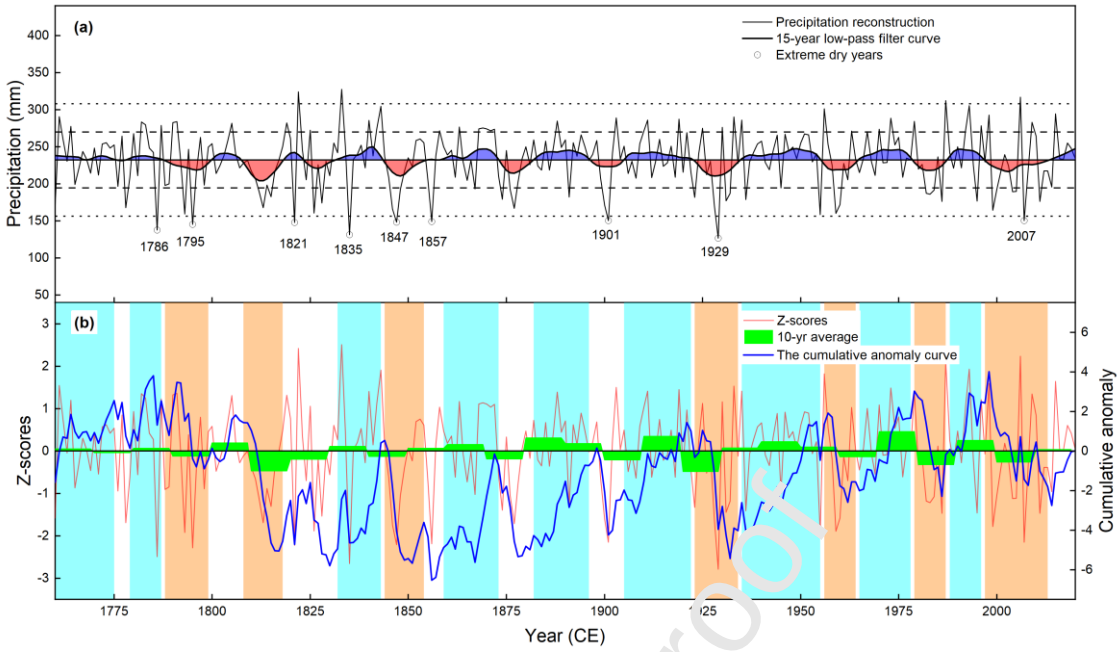

Fig. 4. (a) The reconstructed total March-June precipitation and the 15-year low-pass filter curve since 1760 CE. The horizontal middle line presents the average reconstructed precipitation. The horizontal dotted lines represent one SD, and the horizontal outer lines represent two SDs. (b) Standardized index of reconstructed precipitation and the analysis of the cumulative anomaly curve. The green squares represent the 10-year average. The cyan shadows represent the continuous wet periods, and the orange shadows present the continuous dry periods.

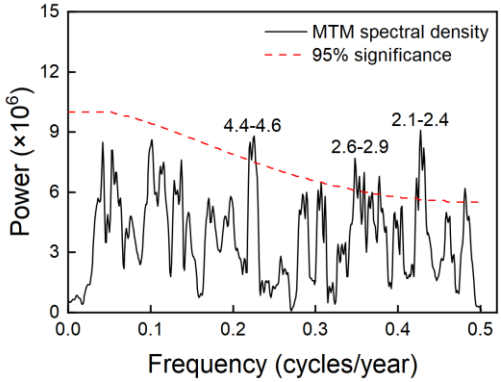

Fig. 5. Principal cycles calculated from the multitaper spectral analysis method

(MTM). The red dotted line presents the 95% significance level.

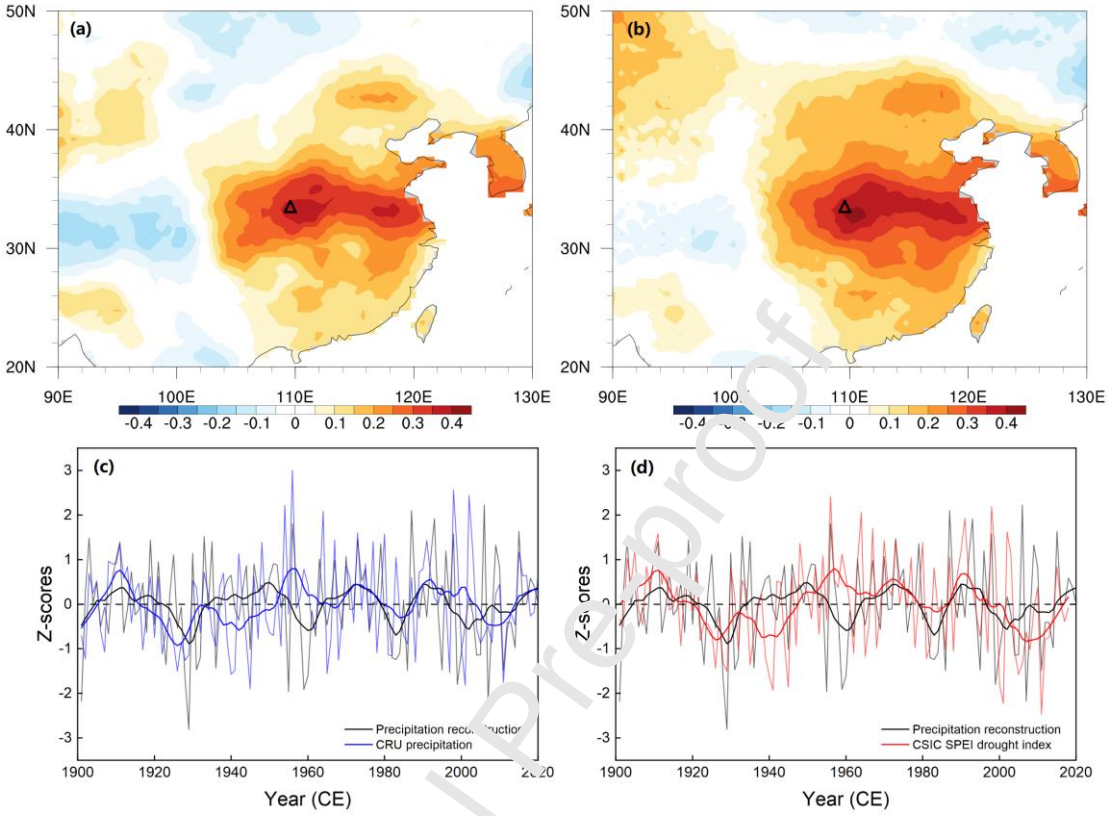

Fig. 6. Spatial correlation patterns of the reconstructed precipitation with the CRU gridded total March-June precipitation (a) and the CSIC gridded mean March-June SPEI (b) since 1901 CE. The triangle indicates the location of the Shangxian meteorological station, the same below. Comparison of reconstructed precipitation with precipitation (c) and SPEI (d) curves, respectively, of the eastern Qinling Mountains and the Yangtze-Huai River Basin (28°-36° N, 108°-118° E). The thin lines represent the original data, and the thick lines correspond to the 10-year low-pass filtered data.

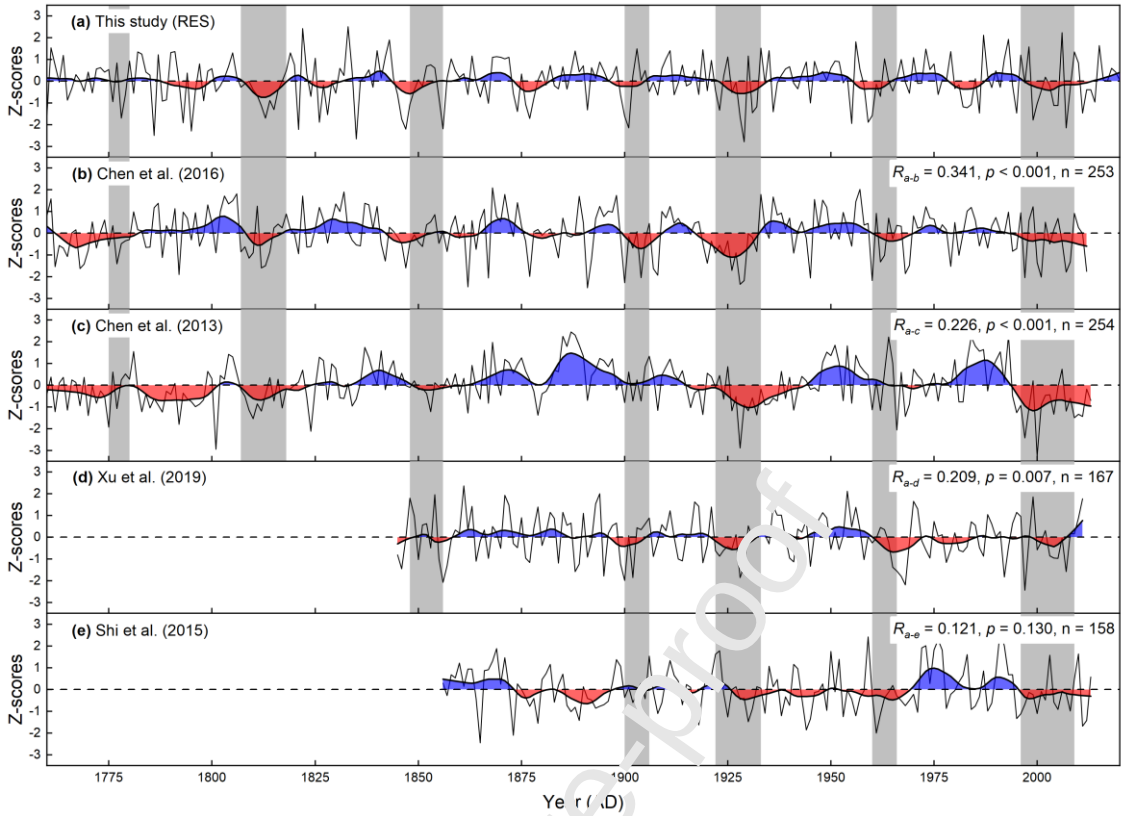

Fig. 7. Comparison of several precipitation reconstructions based on tree-ring records. (a) Precipitation reconstruction from March to June in the Qinling-Bashan mountainous area (this study). (b) Precipitation reconstruction from April to June in Huashan, north-central China (Chen et al., 2014). (c) Precipitation reconstruction from April to July in north-central China (Chen et al., 2013). (d) Early summer (May-June) precipitation reconstruction in the lower Yangtze River basin (Xu et al., 2019). (e) Precipitation reconstruction from February to April in the lower reaches of the Yangtze River, southeastern China (Shi et al., 2015). The thin lines were original, and the thick lines were 15-year low-pass filtered. Shadow area indicate the common dry periods. The correlation coefficients are between the original data.

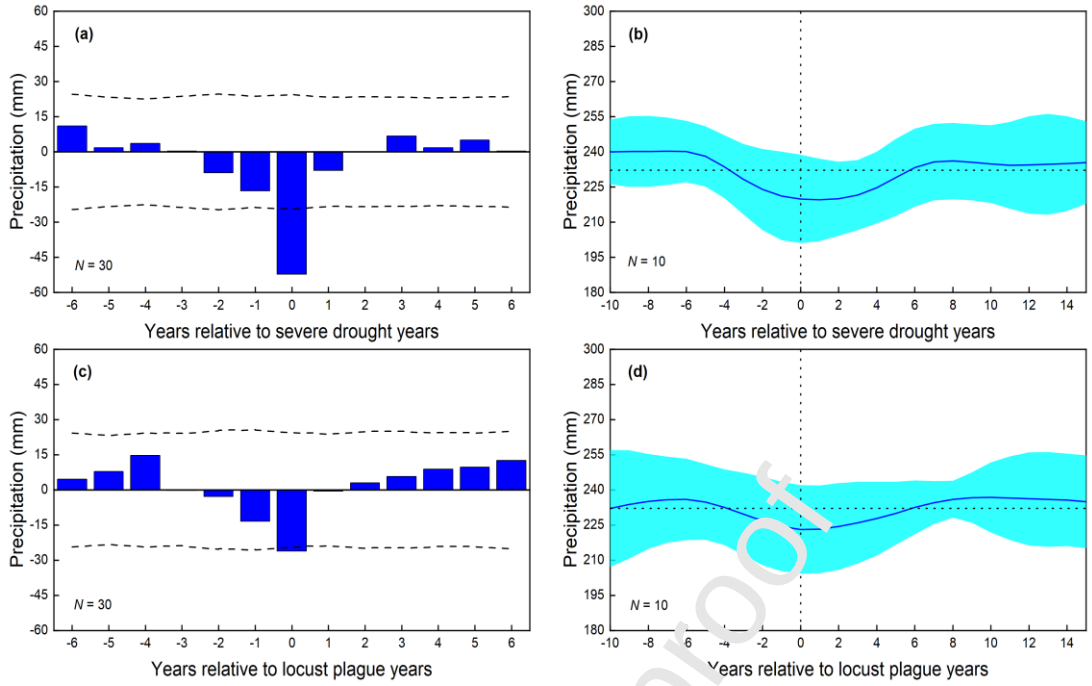

Fig. 8. Results of the superposed epoch analysis (SEA) testing the response of reconstructed precipitation to drought (a) and locust plague (c). The dotted line indicates a 99.9% confidence level. Multidecadal composites of the 10 strongest drought years (b) and 10 strongest locust plague years (d). The multidecadal composites were calculated using 15-year low-pass filtered precipitation, and the shadings represent the 95% confidence interval.

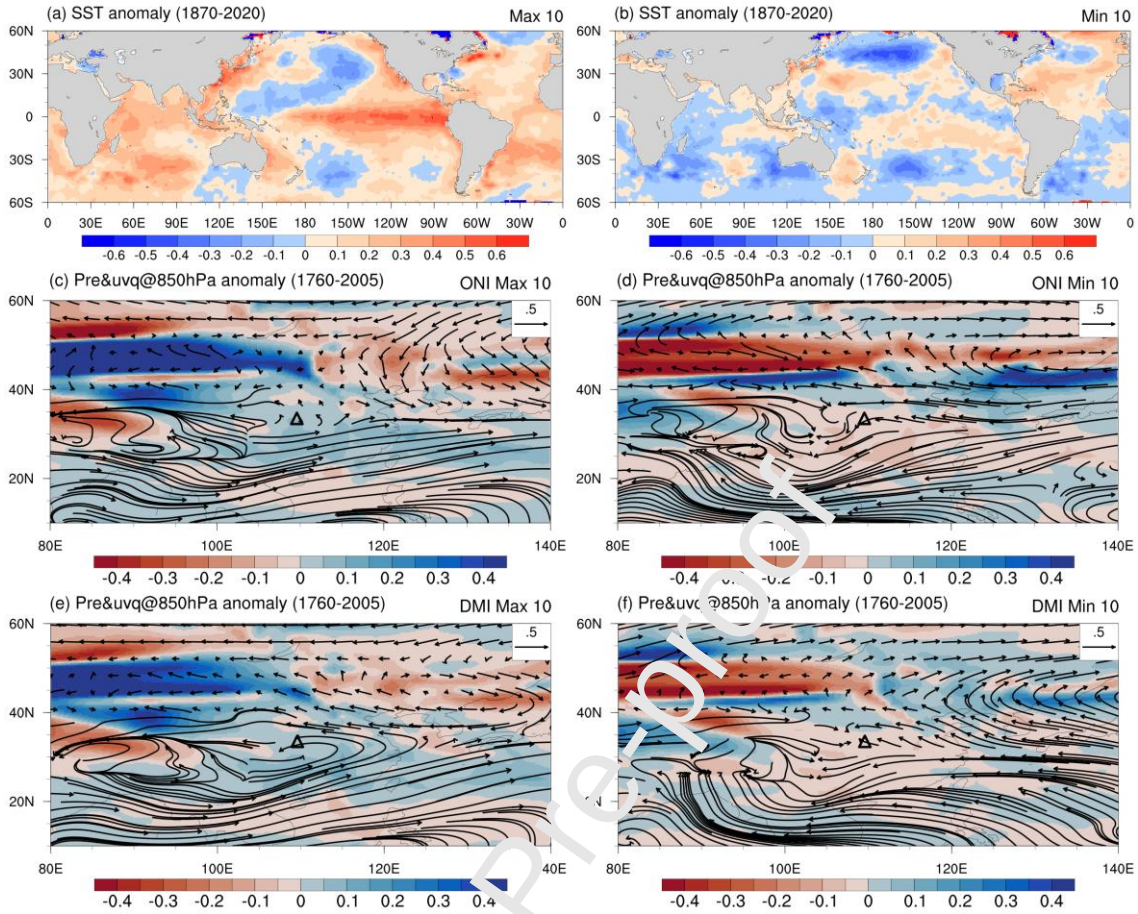

Fig. 9. Composite maps of SST anomalies (°C) for the 10 highest (a) and 10 lowest (b) years from the previous December to the current June during 1870-2020. Spatial patterns of precipitation (shading, mm/day) and 850 hPa water vapor transport anomalies (vectors, where uq and vq are multiplied by 1000) in El Niño (c), La Niña (d), warm IOD (e), and cold IOD (f) years during 1760-2005 in the CESM-LME simulation.

Table 1. Tree-ring sampling sites and meteorological station.

Site	Lat. (N)	Lon. (E)	Elevation (m)	Cores/trees	Species	Peiod
WXS	34.35°	110.36°	1174	41/23	*Pinus bungeana*	1753-2018
DLS	33.76°	110.80°	1499	43/22	*Pinus tabulaeformis*	1959-2018
HPC	32.82°	109.73°	809	49/23	*Pinus bungeana*	1857-2020
Shangxian	33.52°	109.58°	742.2			1955-2016

Table 2. Statistical characteristics of the composite RES chronology.

Statistics item	Value
Mean sensitivity	0.211
Standard deviation	0.215
Signal-to-noise ratio	10.702
Expressed population signal (EPS)	0.915
Variance in first principal component (%)	25.1
Mean correlation among all series	0.688
Year where EPS ≥ 0.85 (number of trees)	1760(10)
Sample size	133/68

Table 3. Statistics of the split verification method for the precipitation reconstruction based on the composite RES chronology.

	Calibration (1955-1985)	Verification (1986-2016)	Calibration (1985-2016)	Verification (1955-1985)
r_1	0.560**	0.709**	0.709**	0.560**
R^2	0.314	0.502	0.502	0.314
r_2		0.827**		0.670**
PMT		5.527		4.572
F		29.236**		13.283**
RE		0.501		0.314
CE		0.473		0.286

Note: r_1 is the correlation coefficient from the leave-one-out cross validation; R^2 is the model explained variance; r_2 is the correlation coefficient of the first difference; PMT is the product means test; F is the F test of the regression models; RE is the reduction of error; CE is the average coefficient of efficiency; ** indicates the 99% confidence level.

Table 4. Summary characteristics of the total March-June precipitation reconstruction.

Wet periods	Mean(mm)	Dry periods	Mean(mm)
1760-1775	238.21	1788-1799	222.76
1779-1787	239.73	1808-1818	211.10
1832-1843	249.90	1844-1854	218.36
1859-1873	243.91	1923-1934	216.30
1882-1896	242.94	1956-1964	227.57
1905-1922	239.52	1979-1987	224.44
1935-1955	238.61	1997-2013	222.61
1965-1978	240.90		
1988-1996	243.44		

Note: A wet period is an interval with filtered precipitation continuously above average for more than 9 years, and a dry period is an interval with filtered precipitation continuously below average for more than 9 years.

Table 5. The precipitation variations in drought and locust plague events.

Event year	Anomaly percentage	Drought	Locust plague	Event year	Anomaly percentage	Drought	Locust plague
1778	-27.7%		Y	1891	-21.5%		Y
1786	-40.6%		Y	1892	10.1%		Y
1788	-14.9%	Y		1900	-26.3%	Y	Y
1792	-0.5%		Y	1901	-35.2%	Y	
1793	-31.4%		Y	1902	4.0%		Y
1802	-3.3%		Y	1915	-3.6%		Y
1803	2.5%		Y	1920	-7.1%	Y	
1813	-27.7%	Y		1923	-21.8%	Y	
1814	-14.5%	Y		1927	-0.7%		Y
1824	-11.5%		Y	1928	-26.9%	Y	Y
1835	-43.4%	Y	Y	1929	-45.5%	Y	Y
1836	0.3%		Y	1930	18.9%	Y	Y
1837	3.3%		Y	1931	-23.8%	Y	Y
1838	8.6%		Y	1932	-19.3%	Y	
1846	-28.4%	Y		1945	-16.3%	Y	
1847	-36.1%	Y	Y	1955	-31.7%	Y	
1856	-35.8%	Y	Y	1959	-30.9%	Y	

1857	2.4%		Y	1960	-25.9%	Y
1858	16.9%		Y	1962	-11.5%	Y
1862	-10.1%		Y	1982	-19.3%	Y
1867	-16.7%	Y		1983	-19.9%	Y
1877	-28.0%	Y	Y	1984	-17.6%	Y
1879	0.8%		Y	1986	-24.0%	Y
1881	-2.8%	Y	Y	1995	-23.9%	Y
1886	-5.9%		Y	1999	-29.1%	Y

Note: Y is the occurrence of the event.

Declaration of Competing Interest

The authors declare that they have no conflict of inerest.

Article Highlights:

- Tree rings provide a precipitation record of Qinling-Bashan mountainous area since 1760 CE.
- Precipitation reconstruction shows close contacts with drought and locust plague events.
- The extreme precipitation may be caused by the large-scale climate forcing, such as ENSO and IOD.